Biosensors and Bioelectronics 50 (2013) 137–142

Contents lists available at SciVerse ScienceDirect

Biosensors and Bioelectronics

journal homepage: www.elsevier.com/locate/bios

Sensitivity improved plasmonic gold nanoholes array biosensor by coupling quantum-dots for the detection of specific biomolecular interactions

Lihong Niu, Ke Cheng, Yangqing Wu, Tian Wang, Qing Shi, Dan Liu, Zuliang Du*

Key Laboratory for Special Functional Materials of Ministry of Education, Henan University, Kaifeng 475004, PR China

ARTICLE INFO

Article history:
Received 13 March 2013
Received in revised form
28 May 2013
Accepted 10 June 2013
Available online 18 June 2013

Keywords:
Large-scale
Nanosphere lithography
Gold nanoholes array
Label-free SPR biosensors
Enhanced detection sensitivity
Quantum dots

ABSTRACT

In this paper, we focused on the large-scale fabrication of gold nanoholes array capable of supporting surface plasmonic resonance (SPR) via the developed nanosphere lithography (NSL) technique, which could be used as high performance biosensor for the detection of specific streptavidin–biotin interactions. Direct UV–vis absorption mode measurement was used to monitor the SPR peak shift. For the better immobilization of biotin, the surface of gold nanoholes array was functionalized with 3-mercaptopropyl trimethoxysilane (MPTS) and 3-aminopropyl triethoxysilane (APTES). After the streptavidin binding to the biotin, the SPR peak position showed an 11 nm wavelength shift due to the refractive index change caused by the biotin–streptavidin binding. The sealing treatment was performed by using bovine serum albumin (BSA) to eliminate the influences of nonspecific adsorption for more accurate detection. Interestingly, the detection sensitivity of the gold nanoholes array could be further enhanced by coupling the water-soluble CdSe/ZnS quantum dots (QDs), which showed four-fold improvement in detection sensitivity as compared to the gold nanoholes array biosensor without the coupling of QDs. The mechanisms for the enhancement of detection sensitivity were also discussed. This would provide new capabilities for the highly sensitive measurements of biomolecular binding.

1. Introduction

The need to probe biomolecular interactions such as biotin/streptavidin binding, antibody/antigen interactions, sugar/lectin interactions, DNA hybridization, and other analyte/receptor interactions is an important motivation for the understanding of fundamental biological processes (Baleviciuteet et al., 2013; Heo et al., 2013; Jin, 2012; Y. Kim et al., 2012; Liu et al., 2013; Tawa et al., 2011; Yao et al., 2011). The fluorescence-based methods have proven to be the most charming platforms suitable for the detection of such biomolecular interactions. However, the complexity and cost have been widely recognized as their inherent shortcomings. Moreover, the label itself may potentially alter the binding properties of biomolecules and cause other significant problems like background binding and autofluorescence (Cooper, 2002; Yang et al., 2008). In contrast, label-free detection methods provide more accurate quantitative and kinetic measurements by monitoring the binding of analytes in their natural forms, which can be realized based on the transduction of plasmonic, optical, electrochemical, or mechanical signals (Sriram et al., 2011; Yanik et al., 2010). Among these label-free biosensing platforms, the SPR is one of the most widely used methods today (Abbas et al., 2011; Law et al., 2011; Park et al., 2010; Pernites et al., 2010). SPR is the optical resonance in electromagnetic radiation due to the coupling with electrons in nanoscale metallic structures. The SPR spectral peak position (λ_{max}) is highly dependent on the local refractive index at the surface of metallic structures. Since the excited surface plasmon modes are very sensitive to the local refractive index changing caused by the binding of specific biomolecules to the metallic structures, it can be used as label-free biosensor with a high sensitivity exceeding 10^3 nm per refractive index unit (RIU) by monitoring the peak shift of λ_{max} (Guo et al., 2010).

In conventional SPR biosensor, light needs to couple to surface plasmon polaritons (SPP) using the Kretschmann configuration, which requires a prism and complicated optical alignment (Hunta and Armani, 2010). In contrast, plasmonic resonances can be excited by direct illumination without any special arrangements for the nanostructured metal films and can be monitored using conventional transmission mode spectroscopy (Nakamoto et al., 2012; Yang et al., 2008). Despite being less sensitive than Kretschmann configuration, the optical transmission configuration enables multiplexed detection and offers better opportunities to develop low-cost biosensor devices with integrated microfluidics for rapid bioanalytical measurements. This significantly simplifies the experimental setup, which is one of the reasons for the increasing popularity of nanostructured SPR

* Corresponding author. Tel./fax: +86 378 3881358.
E-mail address: zld@henu.edu.cn (Z. Du).

0956-5663/$ - see front matter © 2013 Elsevier B.V. All rights reserved.
http://dx.doi.org/10.1016/j.bios.2013.06.023

biosensors. Based on the recent advances in fabrication techniques such as electron beam lithography (EBL), focused ion beam lithography (FIBL), and phase-shifting lithography (PSL), a wide range of patterned metal nanostructures including nanotriangles, nanodisks, nanoholes, bowtie antennas, and nanorings have been fabricated as the SPR based biosensors with high sensitivity (Correia-Ledo et al., 2012; Rodríguez-Fortuño et al., 2011; Sharpe et al., 2008; Yu et al., 2012). Among them, metal nanoholes array can provide smaller foot-print, denser integration, increased potential for multiplexing and simplified collinear optical detection, in which analyte binding is determined directly due to the plasmon-mediated extraordinary optical transmission (EOT) effect (Escobedo et al., 2010). Several groups have shown the potential of such metal nanoholes array for label-free kinetic SPR biosensing. Yu and Golden (2007) adopted EBL to construct 270 nm thick gold nanoholes array and the distribution of cytochrome was characterized by surface enhanced Raman scattering (SERS). Nakamoto et al. (2012) reported the fabrication of gold nanoholes array by nanoimprinting and vacuum deposition, where they obtained the synchronized responses of current and SPR optical signals in association with the redox change of the Os complex. Sharpe et al. (2008) had characterized and demonstrated the production of a nanoholes array detection system through EBL using cortisol as the model analyte. Immunochemical binding interactions have been sensed using a new cortisol-linker-thiol derivative for surface modification.

However, the above patterned metal nanoholes have been fabricated only with a finite area (always tens to hundreds of micrometer square) by using the slow and expensive top-down fabrication method. This would result in a spectrum change due to the significant contribution from the edges. In general, the desirable nanofabrication technique for substrate-bound nanostructures would have some of the conspicuous features, low-cost fabrication, large-area patterning, reproducibility, and tunability of their optical properties (Lee et al., 2011). Therefore, the adequate, large-scale and affordable nanofabrication methods are highly desired for the real application of such nanostructured SPR biosensors. On the other hand, we should note that the SPR resonance mode is always broad for the nanostructured SPR biosensors due to the large absorption in the metal film, which restricts its detection sensitivity and precludes its use for the detection of low surface coverage of bound molecules (Guo et al., 2010). Improving such biosensor's detection sensitivity by new strategy is still the key point for the further advances of the metallic nanostructured SPR biosensors.

In this paper, we focus on the design and large-scale fabrication of gold nanoholes array using the developed NSL technique, which utilizes a hexagonally closely-packed nanosphere mask that permits direct metal deposition onto a substrate through the interstitial regions of the mask. The large-scale feature of the gold nanoholes array allows us to detect the interaction of biomolecules through the direct UV–vis absorption mode measurement. In order to detect the specific affinity reaction of the biotin–streptavidin based on our gold nanoholes array SPR biosensors, the layer-by-layer chemical modification was conducted to make the biomolecule firmly immobilized on the surface of gold nanoholes array. BSA was used to reduce the nonspecific adsorption. The detection sensitivity of the gold nanoholes array biosensor can be further enhanced by coupling the core–shell CdSe/ZnS QDs to streptavidin.

2. Materials and methods

2.1. Large-scale fabrication of gold nanoholes array on the glass substrate

Slides glass substrate was treated by piranha solution (95% H_2SO_4:30% H_2O_2=3:1 by volume) for 30 min to clean the surface. After this, the slides glass substrate was rinsed with ethanol, acetone, and water. Then, it was blow-dried with nitrogen gas. The polystyrene (PS) spheres with a diameter of about 330 nm were synthesized using the surfactant-free emulsion polymerization. The hexagonal closely-packed PS monolayer template was fabricated on the pre-cleaned slides glass substrate using the modified float-transferring technique (Cheng et al., 2012a). In brief, the water/ethanol dispersion containing monodisperse PS spheres was dropped onto the pre-cleaned slides glass. Subsequently, the slides glass was immersed into the water filled Petri dish with a tilt angle of 30–40°. The dispersion spread on the water surface, resulting in a self-assembled PS monolayer film. Then the PS monolayer film was picked up by another slides glass. The diameter of PS spheres was decreased slightly by the reactive ion etching (RIE) treatment (150 W, 15 s) to expand the voids between them. The etched PS monolayer on the slides glass was taken out from the RIE chamber and then thermo-treated at 110 °C for 2 min in order to increase the binding force between the PS spheres and slides glass. The gold deposition was performed at 200 V, 0.2 A for 30 s using a magnetron sputtering system. After the gold sputtering, the PS sphere template was thoroughly removed from the slides glass substrate by dissolution in tetrahydrofuran under a gentle ultrasonic bath for 1 min. Finally, the large-scale gold nanoholes array was obtained on the slides glass substrate. The gold nanoholes array showed a large-scale uniformity as can be seen from Fig. 1a.

2.2. Surface functionalization of gold nanoholes array

The surface of gold nanoholes array was modified for better immobilization of biotin via the layer-by-layer method. Firstly, the gold nanoholes array was immersed into 20 ml solution containing 1% MPTS, 95% methanol, and 4% 1 mM acetic acid for 30 min. Such process resulted in the formation of a silane-terminated MPTS self-assembled monolayer (SAM) on the gold surface. After thoroughly rinsed with water, the slides glass was ultrasonicated in ethanol and water solution successively and was dried by nitrogen gas flow at the room temperature. Secondly, the MPTS modified gold nanoholes array was silanized in APTES solution. In detail, the solution containing 3 ml ultrapure water and 23.5 ml ammonia was added to the other solution containing 25 μl APTES in 23.5 ml absolute ethanol and mixed homogeneously. Subsquently, the MPTS modified gold nanoholes array was immersed into the mixed solution for 15 min. After being taken out from the mixed solution, the gold nanoholes array was thoroughly rinsed with absolute ethanol and dried by nitrogen gas flow.

2.3. Biotin immobilization and bovine serum albumin sealing treatment

Biotin–N-hydroxysuccinimide (biotin–NHS) was anchored onto the surface of functionalized gold nanoholes array via the following process. Firstly, the MPTS and APTES functionalized gold nanoholes array was immersed into the mixed solution of 300 μl biotin–NHS (150 μM) and 29.7 ml phosphate buffer solution (PBS) (pH 7.2, 0.01 M) for 24 h at 4 °C. After this, a large amount of PBS buffer solution and water were used to flush away the unreacted biotin from the gold nanoholes array and dried by nitrogen gas flow. Secondly, the biotin bonded to the gold nanoholes array was sealing treated in order to eliminate the influences of nonspecific adsorption for the more accurate detection. In detail, the antibody immobilized gold nanoholes array was immersed into the solution consisting of 300 μl BSA (1 mg ml^{-1}) and 29.7 ml PBS (pH 7.2, 0.01 M) for 30 min. Finally, nitrogen gas dried sample was placed into the mixed solution containing 500 μl streptavidin and 4.5 ml

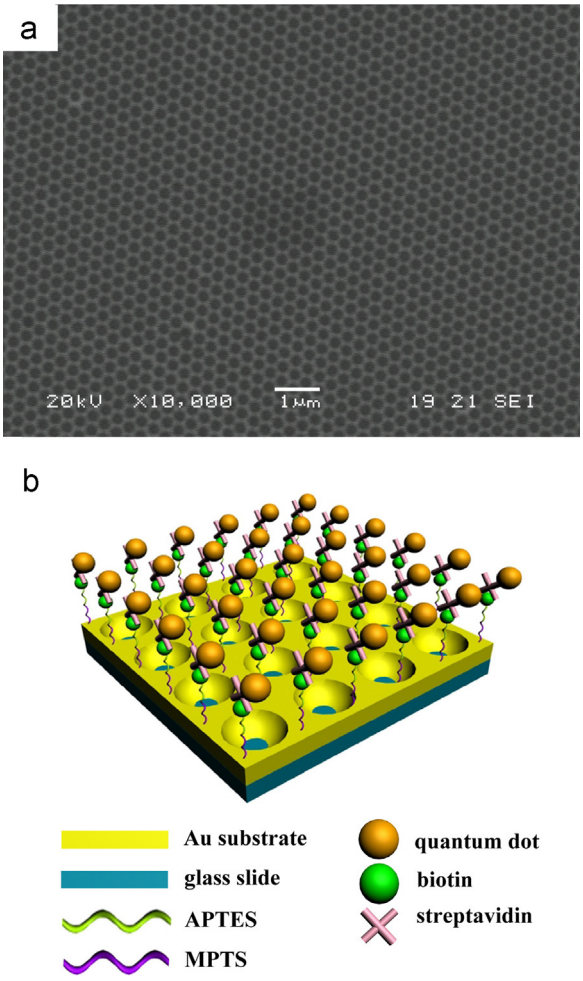

Fig. 1. (a) The SEM image of large-scale gold nanoholes array, and (b) schematic diagram of the gold nanoholes array biosensor coupling with QDs for the detection of biotin–streptavidin interactions.

PBS for 6 h at 4 °C in order to identify the streptavidin target molecules.

2.4. Coupling the QDs with streptavidin to enhance the detection sensitivity

In order to further enhance the detection sensitivity of the gold nanoholes array, the water-soluble core–shell CdSe/ZnS QDs were coupled with the streptavidin target molecules. The aqueous fluorescent CdSe/ZnS QDs were prepared by a versatile phase transfer method (Shen et al., 2009; Zhou et al., 2011), where amphiphilic oligomer (polymaleic acid *n*-hexadecanol ester, PMAH) was used as surface coating agents. The resulting PMAH–CdSe/ZnS QDs can be readily redispersed into water, which is suitable for the coupling of streptavidin target molecules. In detail, the pretreated CdSe/ZnS QDs were added to the 200 μl of streptavidin (2.5 μM) in PBS and reacted for 3 h. The final products were centrifuged and the sediments were redispersed into PBS. In order to confirm the formation of chemical bonds between streptavidin and CdSe/ZnS QDs, the Fourier transform infrared spectroscopy (FTIR) measurement was carried out as shown in Fig. S1. The characteristic peak at 1655 nm could be assigned to the C=O stretching vibration of amide I, which indicated that the carboxyl group of QDs could react with the amino group of streptavidin via the amidation. Finally, the BSA sealing treated gold nanoholes array was immersed into the mixed solution of 200 μl CdSe/ZnS QDs coated streptavidin solution and 3 ml PBS to react for 14 h. Fig. 1b shows the schematic illustration of the gold nanoholes array biosensor used to detect the specific reaction between biotin and streptavidin.

3. Results and discussions

3.1. The atomic force microscopy images of gold nanoholes array under different treatments

Fig. 2 shows the atomic force microscopy (AFM) images of gold nanoholes array under different treatments. Fig. 2a is the AFM image of as-prepared gold nanoholes array, which shows perfect continuous nanoholes with a large area. The depth and diameter of the nanoholes were about 20 nm and 300 nm, respectively. The surface of the gold nanoholes array was quite rough which facilitated to treat the surface for anchoring the biomolecules. Electrostatic interaction or macromolecular adsorption was frequently adopted for the binding between the biomolecules and gold surface. However, such physical modification approaches usually could not offer a strong binding force between biomolecules and the substrate, which would lead to the desorption of biomolecules. In contrast, immobilizing the biomolecules via chemical bonds was superior to the physical modification approaches since the chemical binding is usually stronger. Aimed at this, the gold surface was modified via MPTS and APTES for better immobilization of the biotin in our case. The AFM image of MPTS treated gold nanoholes array is shown in Fig. 2b. The height of the gold nanoholes was about 20 nm after the MPTS treatment, which is almost the same as that of the untreated gold nanoholes array as can be seen from Fig. 2d and e. When the gold nanoholes array was further treated by APTES, the height of the gold nanoholes increased to about 50 nm as shown in Fig. 2f. However, we should note that the absolute height observed in Fig. 2f depends on the value of the highest point in the film, which cannot illustrate the real film thickness of MPTS and APETS. Therefore, the root mean square (rms) values are analyzed as shown in Fig. S2, which are 4.427 nm, 5.081 nm and 7.055 nm for the untreated, MPTS treated and APTES treated gold nanoholes array, respectively. The variations in the rms values suggested the formation of MPTS and APTES monolayer on the surface of gold nanoholes array. In fact, the formation of double layer SAMs of MPTS and APTES on the surface of the gold substrate had been proved by Zhang (2008) through AFM and electrochemical impedance spectroscopy measurements.

In order to further confirm the formation of direct chemical bonds during the MPTS and APTES functionalization processes, X-ray photoelectron spectroscopy (XPS) was conducted as shown in the supplementary information. The XPS results confirmed that MPTS could be self-assembled on the surface of the gold nanoholes array via the Au–S bond as shown in Fig. S3. While, the observed binding energy (BE) of 532.3 eV for the Si–O–Si bonds confirmed the formation of chemical bonds between the MPTS and the APTES through the dehydration reaction as shown in Fig. S4. By the APTES treatment, an amino-contained SAM could be formed, which facilitated the combination of biotin–NHS. Indeed, a BE of 288.1 eV in the C(1s) region for the Au–MPTS/APTES/biotin is observed as shown in Fig. S5, which could be assigned to the N–C=O bonds. The formation of N–C=O bonds indicated that the biotin could chemically bind to the APTES via the amidation reaction.

3.2. Detection of the biotin–streptavidin binding through the UV–vis spectroscopy

The UV–vis absorption spectra of normally incident white light through the gold nanoholes array with biotin–streptavidin binding are shown in Fig. 3a. The concentration of streptavidin was

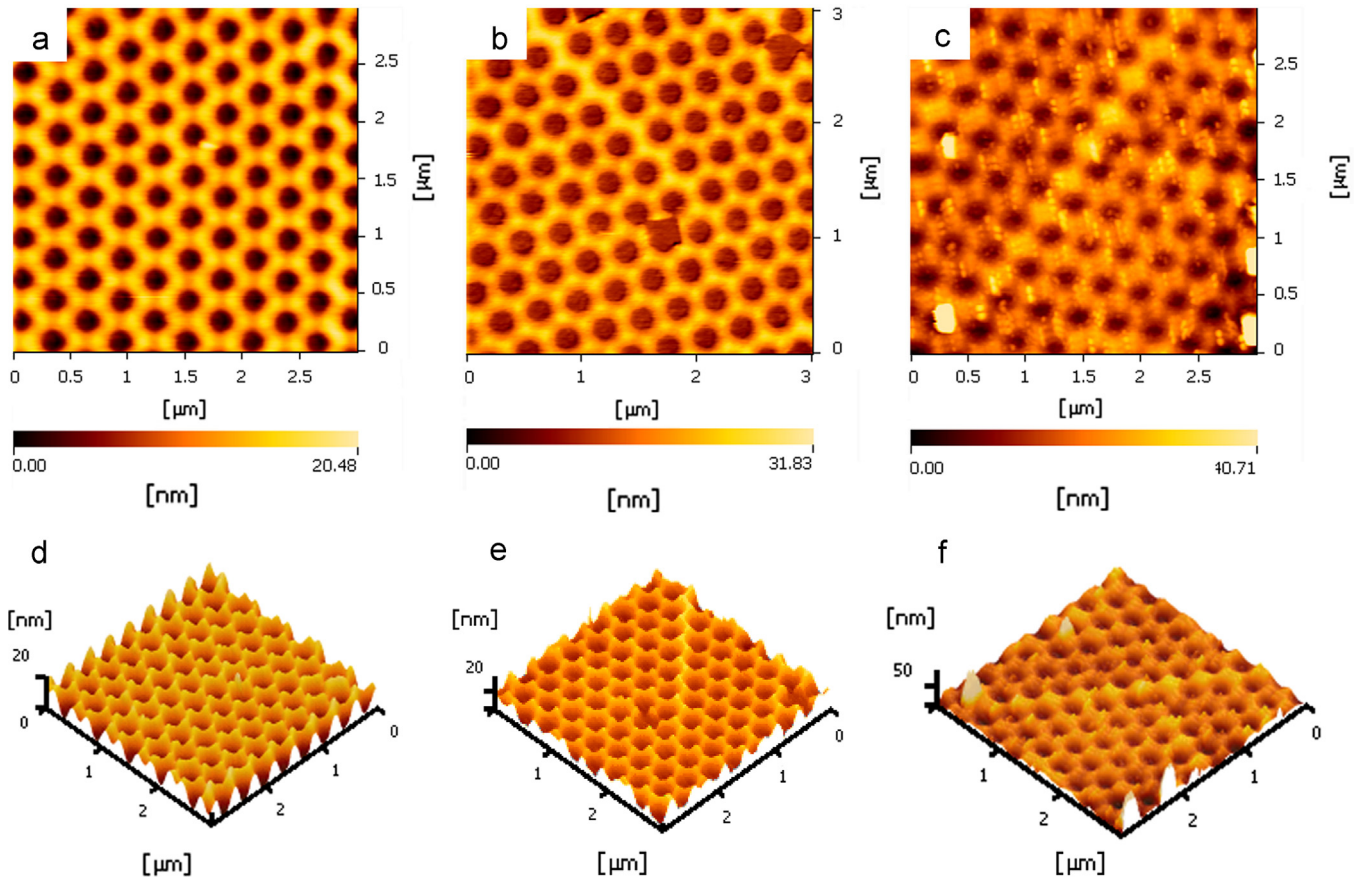

Fig. 2. AFM images of gold nanoholes array: (A) untreated, (B) treated by MPTS and (C) further treated by APTES. Bottoms are the corresponding 3D AFM images.

250 nM. The UV–vis spectrum of gold nanoholes array exhibited an absorption peak at around 755 nm, which originated from the interactions between the incident light and the SPR generated on the surface of gold nanoholes array. The SPR related absorption peak depended on the array periodicity, film thickness, hole size, and hole shape. And the underlying physical mechanisms have been studied by many research groups (Cheng et al., 2012a, 2012b). No obvious SPR peak shift could be observed for the MPTS, APTES surface functionalization and the subsequent biotin anchored processes as shown in Fig. S6. However, the SPR peak shifted to longer wavelengths when streptavidin was introduced. As we know, the excited surface plasmonic modes are very sensitive to the change of local refractive index (Liang et al., 2012; Wang et al., 2011). Therefore, the 14 nm wavelength shift could be attributed to the change of the local refractive index induced by both the specific binding of streptavidin with biotin and nonspecific physical adsorption of streptavidin.

Distinguishing the nonspecific binding of streptavidin on the surface of plasmonic sensor was crucial for the more accurate detection of biotin–streptavidin binding in the label-free sensing technique. In order to do so, the biotin bonded to the gold nanoholes array was sealing treated with BSA. The BSA can fulfill the passivation to those areas without biotinylation, which would avoid the possible electrostatic adsorption (nonspecific physical absorption) of streptavidin. The UV–vis absorption spectrum after the BSA sealing treatment is shown in Fig. 3b. Compared to the 14 nm wavelength shift observed in Fig. 3a, only an 8 nm wavelength shift could be obtained. The smaller wavelength shift indicated there were some nonspecific adsorptions of streptavidin through the electrostatic interaction or macromolecular adsorption. And the BSA sealing treatment could prohibit such nonspecific binding effectively. Additional control experiment was conducted, wherein the immunoglobulin G (IgG) from egg white was used as target analyte instead of streptavidin. No obvious wavelength shift could be observed as shown in Fig. S6, which further confirmed the ability of our gold nanoholes array for the detection of specific biotin–streptavidin interactions.

3.3. Enhanced detection sensitivity of gold nanoholes array by the coupling of CdSe/ZnS QDs

In order to improve the detection sensitivity of metallic nanostructured SPR biosensors, several methods have been proposed. Rational design of metallic nanostructures can lead to the improvements of detection sensitivity via narrowing the spectral linewidths and hence reducing the standard deviation of measured λ_{max} (Hunta and Armani, 2010). This provided an effective way to improve the sensitivity of SPR biosensors for the detection of analytes. Coupling of inorganic semiconducting emitters was another effective strategy to improve the sensitivity of SPR biosensors. Van Duyne et al. demonstrated that using antibody-labeled gold nanoparticles bound on the surface of inorganic nanoparticles can dramatically increase the observed response from localized surface plasmonic resonance (LSPR) sensors (Hall et al., 2011). Oh et al. (2005) used streptavidin-labeled QDs and biotin-labeled Au nanoparticles to measure avidin based on an energy transfer quenching signal transduction from the inhibition assay. Compared to the coupling of gold nanoparticles, QDs are optically robust and they present tunable emission bands and greater flexibility in terms of excitation. In our present work, the water-soluble core–shell CdSe/ZnS QDs were used to couple with the streptavidin target biomolecules in order to improve the detection sensitivity of our gold nanoholes array.

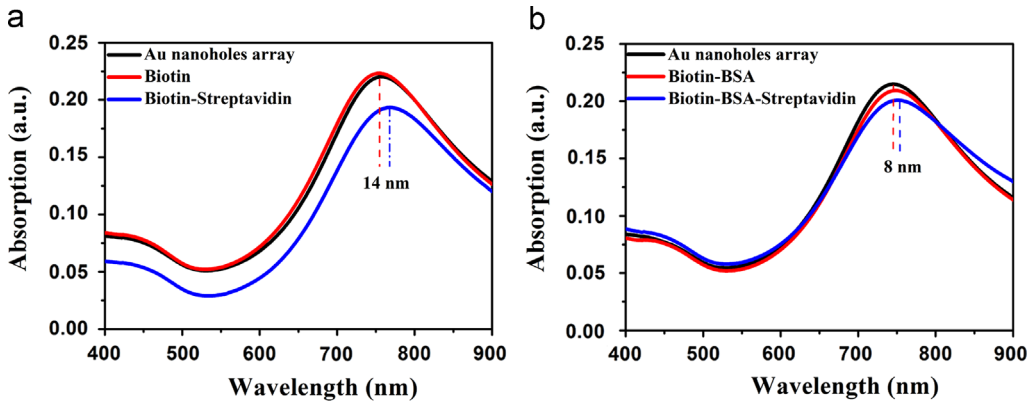

Fig. 3. UV–vis spectra of streptavidin binding to biotin on the surface of the modified gold nanoholes array (a) without the BSA sealing treatment, and (b) with the BSA sealing treatment.

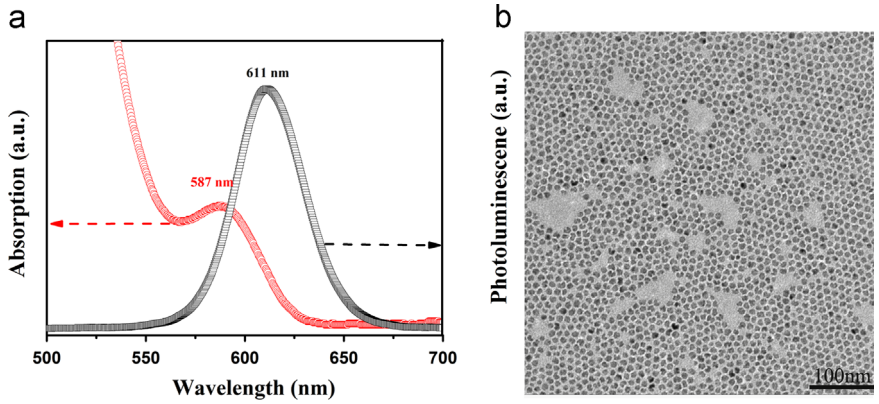

Fig. 4. (a) UV–vis and photoluminescence spectra of core–shell CdSe/ZnS QDs, and (b) the TEM image of core–shell CdSe/ZnS QDs.

Fig. 4a shows the absorption and photoluminescence (PL) spectra of the water-soluble core–shell CdSe/ZnS QDs, which exhibits a clear excitation absorption peak at about 587 nm. The PL emission of the CdSe/ZnS could be precisely tuned in the visible range from 515 nm to 760 nm by changing the ratio of chemical components, while the particle sizes were almost unvaried (Zhou et al., 2011). The CdSe/ZnS QDs with red emission at 611 nm were chosen to couple the streptavidin here. A typical transmission electron microscopy (TEM) image of the CdSe/ZnS QDs is shown in Fig. 4b. The QDs have an average diameter of 10 nm, and are monodisperse. No obvious shape change and particle aggregation could be observed from the TEM image. Interestingly, the SPR peak shifted to the longer wavelengths by about 30 nm after the coupling of streptavidin with core–shell CdSe/ZnS QDs as shown in Fig. 5. The SPR peak shift improved about four-fold compared to the wavelength shift of 8 nm without the coupling of QDs. In order to exclude the larger SPR peak shift caused by the introduction of CdSe/ZnS QDs, the QDs were used as target analyte solely without the streptavidin. No obvious wavelength shift could be observed as shown in Fig. S7. Therefore, the larger wavelength shift observed in Fig. 5 could be attributed to the enhanced sensitivity for the specific detection of biotin–streptavidin interactions. As we know, the theoretical maximum response R_{max} can be calculated using the formula (Guo et al., 2010):

$$R_{max} = \frac{M_{analyte}}{M_{ligand}} R_{ads} n$$

where R_{max} is the spectral shift in our case, $M_{analyte}$ and M_{ligand} are the molecular weights of the analyte and the ligand, R_{ads} is the sensor response of the ligand adsorbed on the surface, and n is the molar ration of the binding sites. We can see that the R_{max} is proportional to the binding sites n, which indicates that the R_{max} depends on the amount of streptavidin bonded to the sensing surface. As we know, each biotin molecule can only link one streptavidin molecule. The number of streptavidin molecules bonded to the sensing surface are limited to the available binding sites of biotin. There are many activated carboxyl groups coated on the 10 nm QDs we used, which indicated more than one streptavidin molecule can bind to the surface of single QD via the

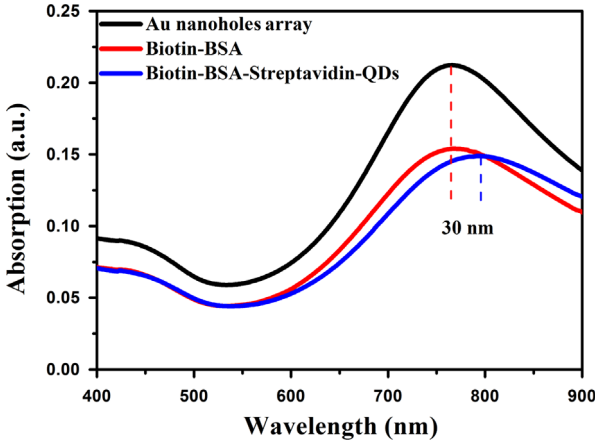

Fig. 5. UV–vis spectra showed the enhanced detection sensitivity of gold nanoholes array by coupling the QDs with streptavidin.

activated carboxyl groups. Therefore, the introduction of QDs can increase the quantities of streptavidin bonded to the sensing surface effectively. The additional streptavidin binding to the surface of QDs would result in additional refractive index changing and then give a contribution for the increased spectral shift as can be seen from Fig. 5.

Another possible reason for the enhanced detection sensitivity was the interactions of emissions from core–shell CdSe/ZnS QDs with the SPR modes of our gold nanoholes array. As we know, such interactions can be realized by controlling the spectral overlap of the plasmonic resonance of metal nanostructures with the absorption and emission spectra of the QDs (Munechika et al., 2011). In fact, the QDs-metal nanostructured system have been widely used to modulate the photoluminescence properties of QDs by the SPR effects of metal nanostructures. K. Kim et al. (2012) used the near-field interactions among QDs and metal nanoparticles to regulate the fluorescence resonance energy transfer (FRET) in the hybrid assemblies of diblock copolymer micelles, QDs, and dyes. In our case, the SPR spectral of gold nanoholes array partially overlapped with the absorption and emission spectra of core–shell CdSe/ZnS QDs as shown in Figs. 4a and 5. The excited-state energy of CdSe/ZnS QDs could be transferred to the gold nanoholes array and coupled with the SPR modes through the empirical nanometal surface energy transfer (NSET) mechanism (Singh and Strouse, 2010). The energy transfer from the QDs to the gold nanoholes array resulted in electron–hole pairs formations (polaritons). Such phenomenon have been observed by Gontijo et al. They observed that the decay rate of excitons in InGaN QWs was increased by a factor of 55 at the proximity of ultrathin silver layer due to the direct transfer of energy into the SPR modes (Gontijo et al., 1999). Such an energy transfer from CdSe/ZnS QDs in our case may strengthen the SPR effects of the gold nanoholes array. Then, an enhanced detection sensitivity of gold nanoholes array could be obtained by coupling the core–shell CdSe/ZnS QDs with streptavidin in the present work.

4. Conclusions

In this paper, we presented the design and large-scale fabrication of gold nanoholes array using the developed NSL technique. It exhibited a SPR related peak at about 710 nm, which could be used as a SPR based biosensor for the detection of the specific biotin–streptavidin interactions. The UV–vis spectrum showed 11 nm wavelength shifts due to the biotin–streptavidin binding, which caused a change of local refractive index. In order to improve the detection accuracy, the sealing treatment was performed using BSA to eliminate the influences of nonspecific adsorption. In addition, the detection sensitivity of the gold nanoholes array could be further enhanced by coupling the water-soluble CdSe/ZnS QDs. The SPR peak shifted to the longer wavelengths by 30 nm, which showed a nearly four-fold sensitivity improvement than the gold nanoholes array biosensor without the QDs coupling. The mechanisms of the sensitivity enhancement were attributed to the increased binding sites and the interactions of QDs with the SPR modes through the NSET mechanism. The two important findings of this study were that (1) the SPR based gold nanoholes array biosensor could be fabricated using the NSL technique and (2) the detection sensitivity could be greatly improved by coupling the QDs into the SPR based biosensor, which opened up the possibility of producing low-cost, portable biosensors for highly sensitive detection of biomolecules.

Acknowledgments

This work was supported by Program for Changjiang Scholars and Innovative Research Team in University (No. PCS IRT1126) and the National Natural Science Foundation of China (Nos. 11274093 and 61240053).

Appendix A. Supporting information

Supplementary data associated with this article can be found in the online version at http://dx.doi.org/10.1016/j.bios.2013.06.023.

References

Abbas, A., Linman, M.J., Cheng, Q., 2011. Biosensors and Bioelectronics 26, 1815–1824.
Baleviciuteet, I., Balevicius, Z., Makaraviciute, A., Ramanaviciene, A., Ramanavicius, A., 2013. Biosensors and Bioelectronics 39, 170–176.
Correia-Ledo, D., Gibson, K.F., Dhawan, A., Couture, M., Vo-Dinh, T., Graham, D., Masson, J.F., 2012. Journal of Physical Chemistry C 116, 6884–6892.
Cooper, M.A., 2002. Drug Discovery 1, 515–528.
Cheng, K., Cui, Z.G., Li, Q.Q., Wang, S.J., Du, Z.L., 2012a. Nanotechnology 23, 425303–425309.
Cheng, K., Wang, S.J., Cui, Z.G., Li, Q.Q., Dai, S.X., Du, Z.L., 2012b. Applied Physics Letters 100, 253101–253104.
Escobedo, C., Brolo, A.G., Gordon, R., Sinton, D., 2010. Analytical Chemistry 82, 10015–10020.
Gontijo, I., Boroditsky, M., Yablonovitch, E., 1999. Physical Review B 60, 11564–11567.
Guo, Y.B., Ye, J.Y., Divin, C., Huang, B.H., Thomas, T.P., Baker, J.R., Norris, T.B., 2010. Analytical Chemistry 82, 5211–5218.
Hunta, H.K., Armani, A.M., 2010. Nanoscale 2, 1544–1559.
Hall, W.P., Ngatia, S.N., Duyne, R.P.V., 2011. Journal of Physical Chemistry C 115, 1410–1414.
Heo, S., Kim, K., Christophe, R., Yoon, T.Y., Cho, Y.H., 2013. Biosensors and Bioelectronics 42, 106–111.
Jin, Y.D., 2012. Advanced Materials 24, 5153–5165.
Kim, Y., Chung, K., Lee, W., Kim, D.H., Kim, D., 2012. Applied Physics Letters 101, 233701–233705.
Kim, K., Kim, J., Kim, H., Laquai, F., Arifin, E., Lee, J., Yoo, S., Sohn, B., 2012. ACS Nano 6, 5051–5059.
Law, W.C., Yong, K.T., Baev, A., Prasad, P.N., 2011. ACS Nano 5, 4858–4864.
Lee, S.W., Lee, K., Ahn, J., Lee, J., Kim, M., Shin, Y., 2011. ACS Nano 5, 897–904.
Liang, Y.H., Chang, C.C., Chen, C.C., Chu-Su, Y., Lin, C.W., 2012. Clinical Biochemistry 45, 1689–1693.
Liu, X., Ouyang, L., Cai, X.H., Huang, Y.Q., Feng, X.M., Fan, Q.L., Huang, W., 2013. Biosensors and Bioelectronics 41, 218–224.
Munechika, K., Chen, Y., Tillack, A.F., Kulkarni, A.P., Plante, I.J., Munro, A.M., Ginger, D.S., 2011. Nano Letters 11, 2725–2730.
Nakamoto, K., Kurita, R., Niwa, O., 2012. Analytical Chemistry 84, 3187–3191.
Oh, E., Hong, M., Lee, D., Nam, S., Yoon, H.C., Kim, H., 2005. Journal of the American Chemical Society 127, 3270–3271.
Pernites, R.B., Ponnapati, R.R., Advincula, R.C., 2010. Macromolecules 43, 9724–9735.
Park, D.K., Kim, H.I., Kim, J.P., Park, J.S., Lee, S.Y., Yang, S., Lee, J., Chung, C.H., Sim, S.J., Yoo, P.J., 2010. Langmuir 26, 6119–6126.
Rodríguez-Fortuño, F.J., Martínez-Marco, M., Tomás-Navarro, B., Ortuño, R., Martí, J., Martínez, A., Rodríguez-Cantó, P.J., 2011. Applied Physics Letters 98, 133118–133121.
Sharpe, J.C., Mitchell, J.S., Lin, L., Sedoglavich, N., Blaikie, R.J., 2008. Analytical Chemistry 80, 2244–2249.
Shen, H.B., Wang, H.Z., Tang, Z.J., Niu, J.Z., Lou, S.Y., Du, Z.L., Li, L.S., 2009. CrystEngComm 11, 1733–1738.
Singh, M.P., Strouse, G.F., 2010. Journal of the American Chemical Society 132, 9383–9391.
Sriram, R., Yadav, A.R., Mace, C.R., Miller, B.L., 2011. Analytical Chemistry 83, 3750–3757.
Tawa, K., Umetsu, M., Hattori, T., Kumagai, I., 2011. Analytical Chemistry 83, 5944–5948.
Wang, J., Song, D., Wang, L., Zhang, H., Zhang, H.Q., Sun, Y., 2011. Sensors and Actuators B: Chemical 157, 547–553.
Yu, Q.M., Golden, G., 2007. Langmuir 23, 8659–8662.
Yang, J.C., Ji, J., Hogle, J.M., Larson, D.N., 2008. Nano Letters 8, 2718–2724.
Yanik, A.A., Huang, M., Kamohara, O., Artar, A., Geisbert, T.W., Connor, J.H., Altug, H., 2010. Nano Letters 10, 4962–4969.
Yao, J., Le, A., Schulmerich, M.V., Maria, J., Lee, T., Gray, S.K., Bhargava, R., Rogers, J.A., Nuzzo, R.G., 2011. ACS Nano 5, 5763–5774.
Yu, C.C., Ho, K.H., Chen, H.L., Chuang, S.Y., Tseng, S.C., Su, W.F., 2012. Biosensors and Bioelectronics 33, 267–273.
Zhang, S.J., 2008. Surface Plasmon Resonance and its Applications to the Probing of Macromolecules on Gold Surfaces. East China Normal UniversityShanghai.
Zhou, C.H., Yuan, H., Shen, H.B., Guo, Y., Li, X.M., Liu, D., Xu, L., Ma, L., Li, L.S., 2011. Journal of Materials Chemistry 21, 7393–7400.